A δ-Doped InGaP/InGaAs pHEMT With Different Doping Profiles for Device-Linearity Improvement

Yueh-Chin Lin, Edward Yi Chang, *Senior Member, IEEE*, Hiroshi Yamaguchi, Wei-Cheng Wu, and Chun-Yen Chang, *Life Fellow, IEEE*

***Abstract*—In this paper, δ-doped InGaP/InGaAs pseudomorphic high-electron-mobility transistors (pHEMTs) with doping-profile modifications are investigated in order to improve the device linearity. The proposed modification was based on the third-order intermodulation distortion (IM3) and the third-order intercept point (IP3) analysis using a simple equivalent circuit of the devices. The correlations of the extrinsic transconductance (Gm) with IM3 and IP3 indicate that the flatness of Gm, as a function of gate-bias causes a lower IM3 level. On the other hand, a high Gm with a flatter Gm distribution results in higher IP3 value for the device. Therefore, doping modifications that improve the flatness of the Gm distribution will also improve the device linearity. Doping modifications in the Schottky layer (Schottky layer doped) and in the channel layer (channel doped) of the conventional δ-doped InGaP/InGaAs pHEMT were investigated. It was also found that extra doping, either in the channel region or in the Schottky layer, improved the flatness of the Gm distribution under different gate-bias conditions. This achieved a lower IM3 and a higher IP3 with a small sacrifice in the peak Gm value. The power performances of these devices were tested at different drain biases. Even though it had the lowest electron mobility among the three different types of devices studied, the channel-doped device demonstrated the best overall linearity performance, the highest IP3 value, the lowest IM3 level, and the best adjacent-channel power ratio under code-division multiple-access modulation.**

***Index Terms*—Channel doping, device linearity, InGaP/InGaAs pseudomorphic high-electron-mobility transistor (pHEMT), third-order intercept point (IP3), third-order intermodulation distortion (IM3), δ-doped.**

I. Introduction

MULTICHANNEL transmissions are widely used to transmit signals in modern wireless-communication systems. When there is more than one operating frequency for a system and the neighboring frequencies are located closely to each other, the device used in such a system will generate intermodulation distortion. Among all the types of intermodulation distortions incurred by such devices, third-order intermodulation distortion (IM3) is the most dominant. Thus, it determines the linearity performance of a device. Therefore, IM3 has become the most important factor with devices used in modern wireless-communication systems.

InGaP/InGaAs pHEMTs have been widely used in various high-performance wireless-communication systems [1], [2]. They were very popular because the InGaP Schottky layer unlike the conventional AlGaAs layer does not form a deep-complex center at the desired doping level. Moreover, high-etch selectivity between the InGaP and GaAs materials results in better control during the device-fabrication process [3]. Consequently, this paper examines the δ-doped InGaP/InGaAs pseudomorphic high-electron-mobility transistor (pHEMT) with extra doping at the Schottky layer (Schottky layer doped) and the channel region (channel doped) in order to improve device linearity.

For the assessment of linearity, a nonlinear transfer-function-based analysis method was used. Previously published results have revealed that, in order to minimize third-order distortion, the transconductance needs to remain constant during the operating range of the gate bias. Hence, an improvement in the flatness of the extrinsic-transconductance (Gm) profile should result in lower IM3 levels and a higher third-order intercept point (IP3) and, thus, improve the device linearity [4]. Equation (1) shows the relationship between Gm and the drain-to-source current $(I_{\rm DS})$. To maintain a constant Gm with different gate-to-source voltages $(V_{\rm GS})$, the $I_{\rm DS}$ as a function of $V_{\rm GS}$ should be constantly rising and the $I_{\rm DS}$ value should be large

$$\mathrm{Gm} = \frac{dI_{\rm DS}}{dV_{\rm GS}}. \tag{1}$$

Because $I_{\rm DS}$ is proportional to the electron density, extra doping in the conventional InGaP/InGaAs pHEMT structure was used to modify the $I_{\rm DS}$ and to improve the Gm profile in this paper. The structure of a δ-doped InGaP/InGaAs pHEMT is shown in Fig. 1. Two Si-planar-doped layers with doping concentrations of $4 \times 10^{12}/\mathrm{cm}^2$ and $2 \times 10^{12}/\mathrm{cm}^2$ were used to supply high carrier concentration in the quantum well at the spacer and channel interfaces. For linearity improvement to occur, light doping in the Schottky layer and in the channel layer were used to improve the flatness of Gm as a function of gate-bias conditions. The concentration level of the extra doping in these layers was $n = 5 \times 10^{17}$ cm^{-3}. However, as indicated in this paper, the extra doping results in a great scatter of impurities and causes a decrease of carrier mobility when compared to that of a conventional δ-doped device,

Manuscript received January 3, 2007; revised April 12, 2007. The review of this paper was arranged by Editor Y.-J. Chan.

Y.-C. Lin, E. Y. Chang, and W.-C. Wu are with the Department of Materials Science and Engineering and Microelectronics and Information Systems Research Center, National Chiao Tung University, Hsinchu 30010, Taiwan, R.O.C. (e-mail: edc@mail.nctu.edu.tw).

H. Yamaguchi is with NTT Basic Research Laboratories, Kanagawa 243-0198, Japan, and also with the Department of Physics, Tohoku University, Sendai 980-8578, Japan.

C.-Y. Chang is with the Department of Electronics Engineering, National Chiao Tung University, Hsinchu 30010, Taiwan, R.O.C.

Color versions of one or more of the figures in this paper are available online at http://ieeexplore.ieee.org.

Digital Object Identifier 10.1109/TED.2007.899398

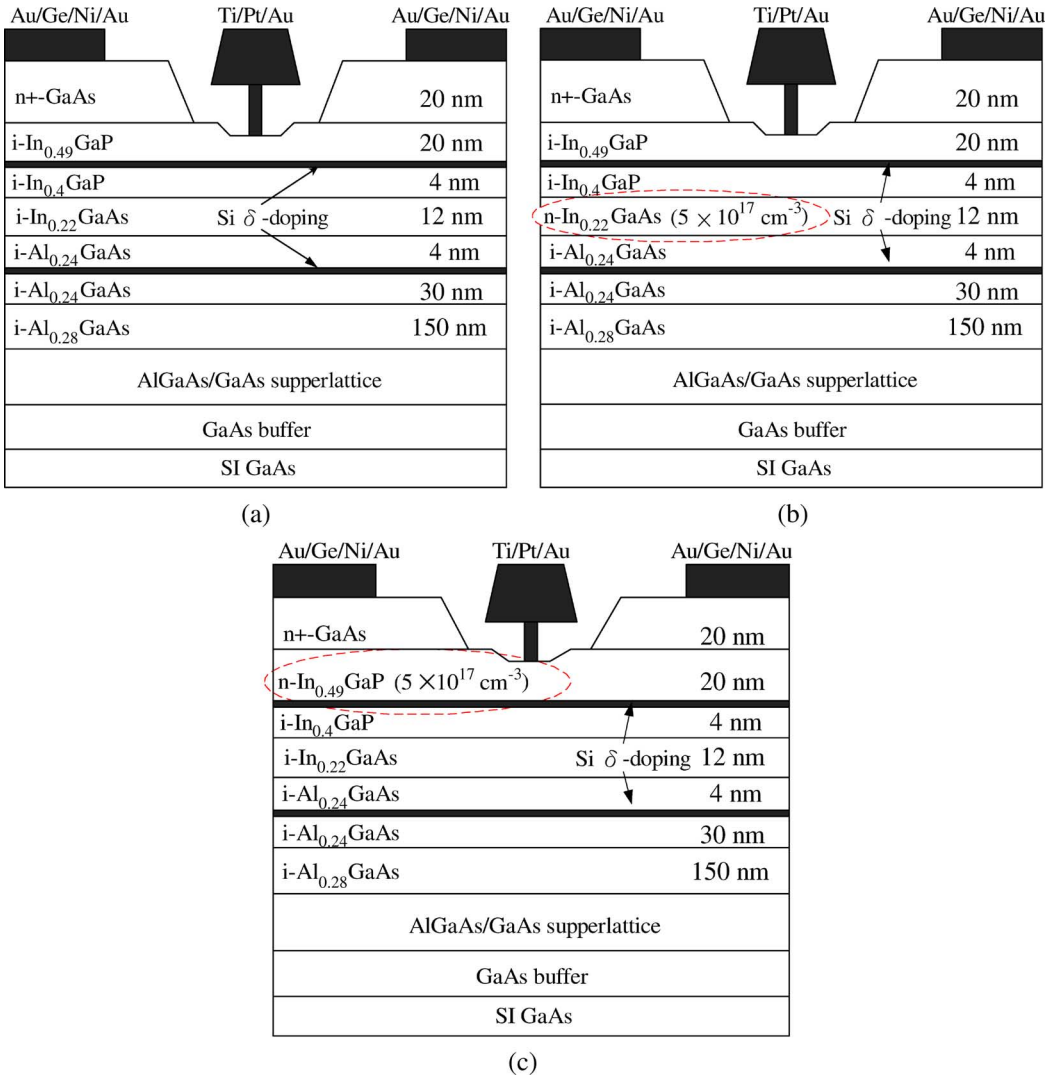

Fig. 1. Structures of the three InGaP/InGaAs pHEMTs in this paper. (a) δ-doped device. (b) Channel-doped pHEMT. (c) Schottky layer-doped pHEMT.

particularly when it is channel-doped [5]. It should be noted that the electron mobility of the channel-doped device in this paper was 3500 $\mathrm{cm}^2/\mathrm{V}\cdot\mathrm{s}$, which was smaller than the Schottky layer-doped device (4100 $\mathrm{cm}^2/\mathrm{V}\cdot\mathrm{s}$) and the conventional δ-doped device (4200 $\mathrm{cm}^2/\mathrm{V}\cdot\mathrm{s}$) due to the impurity scattering in the channel.

II. Device-Linearity Analysis

For device-linearity improvement to occur, a simple device equivalent circuit, as shown in Fig. 2, was used to derivate the relationship between IM3, IP3, and Gm. The nonlinear circuit elements in this model are the Schottky barrier junction capacitance at the gate (C_{gs}), the gate-to-drain capacitance (C_{gd}), the intrinsic transconductance (g_m), and the drain conductance (G_d). Among them, C_{gs} and g_m are dependent on the input voltage (V_i), while Gd is dependent on the output voltage (V_o) [6].

An analysis and estimation of the IM3 level and IP3 value incurred by the device itself began with the derivation of the nonlinear transfer function of the two-port network using

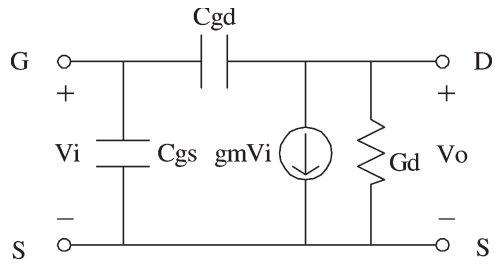

Fig. 2. Simple device equivalent circuit of pHEMT for linearity analysis.

classical theory [7]. In such a case, the device may be classified as a near-linear two-port system with a relatively small amount of nonlinearity. The two port's voltage gain may then be approximated using the polynomial expansion

$$\nu_o = k_1\nu_i + k_2\nu_i^2 + k_3\nu_i^3 + \cdots. \tag{2}$$

Applying Kirchhoff's Current and Voltage Laws at specific nodes in the network, the nonlinear voltage transfer function

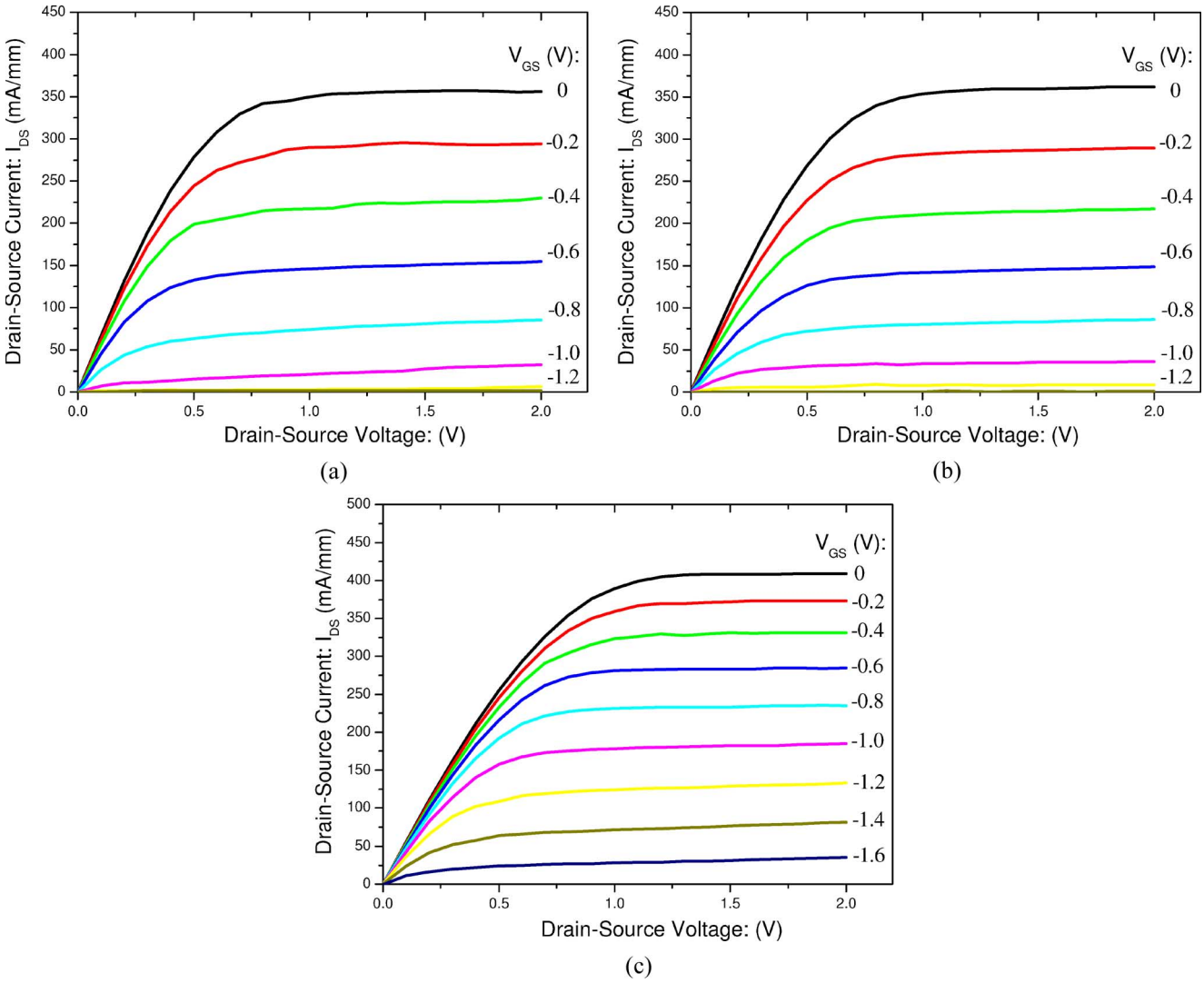

Fig. 3. $I_{\rm DS}$ versus $V_{\rm DS}$ curves for the three different types of 0.25 × 160 μm^2 devices. (a) δ-doped device. (b) Channel-doped pHEMT. (c) Schottky layer-doped pHEMT.

can be derived

$$\nu_o = \left[\frac{j\omega C_{gd}}{G_d} - \frac{g_m}{G_d}\right] \cdot \left[1 + \frac{j\omega C_{gd}}{G_d}\right]^{-1} \nu_i. \tag{3}$$

For the sake of simplicity of analysis, only the first-order significant terms have been considered, the coefficients in (2) can be expressed explicitly as $k_1 = -g_m/G_d$, $k_2 = -g_m'/G_d$, and $k_3 = -(1/2)g_m''/G_d$, where g_m' and g_m'' are the first and second derivatives of the intrinsic transconductance, respectively.

For the analyses of IM3 and IP3, a two-tone signal, which consists of two terminal signals with the same amplitude A at two different but closely located frequencies, is used as the input. Substitution of the two-tone input signal

$$\nu_i = A\cos\omega_1 t + A\cos\omega_2 t \tag{4}$$

into (2) yields the following expression for the IM3 level at frequencies $(2\omega_1 - \omega_2)$ and $(2\omega_2 - \omega_1)$ [7]:

$$\nu_o = \frac{3}{4}k_3A^3\cos(2\omega_1 - \omega_2)t + \frac{3}{4}k_3A^3\cos(2\omega_2 - \omega_1)t. \tag{5}$$

When the load impedance is R_L, the IM3 of the device can be obtained as follows:

$$\begin{aligned}\text{IM3} &= \frac{\left(\frac{3}{4}k_3A^3\right)^2}{2R_L} \\ &= \left(\frac{3}{4\sqrt{2}}\right)^2 \cdot \frac{k_3^2A^6}{R_L} \\ &= \left(\frac{3}{8\sqrt{2}}\right)^2 \frac{(g_m'')^2}{G_{\rm ds}^2 \cdot R_L} \cdot A^6. \end{aligned} \tag{6}$$

By using the IP3 definition (i.e., the linear part is equal to IM3), first, A is obtained using (7), and then, this value is used in the following to obtain the IP3 of device:

$$k_1A = \frac{3}{4}k_3A^3 \tag{7}$$

$$\begin{aligned}\text{IP3} &= \frac{k_1^2A^2}{2R_L} \\ &= \frac{4}{3}\frac{g_m^3}{g_m'' \cdot G_{\rm ds}^2 \cdot R_L}. \end{aligned} \tag{8}$$

In a linear equivalent circuit, the drain–source current model can be used to estimate IM3 and IP3 using the following [8], [9]:

$$i_{\rm ds}(\nu_{\rm gs},\nu_{\rm ds}) = \frac{\partial I_{\rm DS}}{\partial V_{\rm GS}}\cdot\nu_{\rm gs} + \frac{\partial I_{\rm DS}}{\partial V_{\rm DS}}\cdot\nu_{\rm ds} \tag{9}$$

where $\nu_{\rm gs}$ and $\nu_{\rm ds}$ are the incremental gate and drain voltages, respectively. $i_{\rm ds}$ is the linear terms for the drain-to-source current. The small-signal drain-to-source current can be modeled as a function of $V_{\rm GS}$, as shown in the following:

$$\begin{aligned} G_m(V_{\rm GS}) &= \frac{\partial I_{\rm DS}(V_{\rm GS})}{\partial V_{\rm GS}} \\ &= a_1 + 2a_2V_{\rm GS} + 3a_3V_{\rm GS}^2 \\ &\quad + 4a_4V_{\rm GS}^3 + 5a_5V_{\rm GS}^4 + \cdots. \end{aligned} \tag{10}$$

Hence, the relationships between IM3, Gm, and Gds, and IP3, Gm, and Gds are shown in (11) and (12), respectively

$$\text{IM3} \propto \frac{(G_m'')^2}{G_{\rm ds}^2\cdot R_L}\cdot A^6 \tag{11}$$

$$\text{IP3} \propto \frac{(G_m)^3}{G_m''\cdot G_{\rm ds}^2\cdot R_L}. \tag{12}$$

As a result, the IM3 level is directly proportional to the second derivative of the Gm (Gm''), while the IP3 value is inversely proportional to the Gm'' and directly proportional to the third power of Gm. Therefore, a lower IM3 level can be achieved by increasing the flatness of the Gm distribution across the gate-bias region. Meanwhile, a higher value Gm with a flat Gm distribution will result in a higher value IP3. For this reason, extra doping in the Schottky layer and in the channel layer was used to modify the $I_{\rm DS}$ and to increase the flatness of the Gm distribution and, thus, improve the device linearity.

III. Device Fabrication

Three different types of the InGaP/InGaAs pHEMT devices, shown in Fig. 1(a), (b), and (c), were fabricated. There are five major steps in the fabrication of InGaP/InGaAs pHEMT. These include the following: defining the active region, depositing and annealing the ohmic metal, wet chemical etching for gate recess, forming the gate using electron-beam lithography and lift-off process, and gold-plating of the airbridges for the interconnects. The mesa etch was achieved by using $\text{HCl}/\text{H}_2\text{O}$ (1 : 1) solution etching for the InGaP layer and $\text{HF}/\text{H}_2\text{O}_2/\text{H}_2\text{O}$ (2 : 3 : 10) solution for other layers. The ohmic contacts were formed by AuGe/Ni/Au evaporation and were annealed rapidly at 355 °C for 30 s by rapid thermal annealing. A double recess was used to achieve superior device linearity [10]. The gate recess was performed using a highly selective citric acid$/\text{H}_2\text{O}_2/\text{H}_2\text{O}$ solution to selectively remove the cap GaAs material. An $\text{HCl}/\text{H}_2\text{O}$ solution was used to etch the InGaP Schottky layer. The Ti/Pt/Au was then deposited as the Schottky gate metal, and the gate was formed by lift-off technique. The gate length and the source-to-drain spacing on the fabricated devices were 0.25 and 2 μm, respectively.

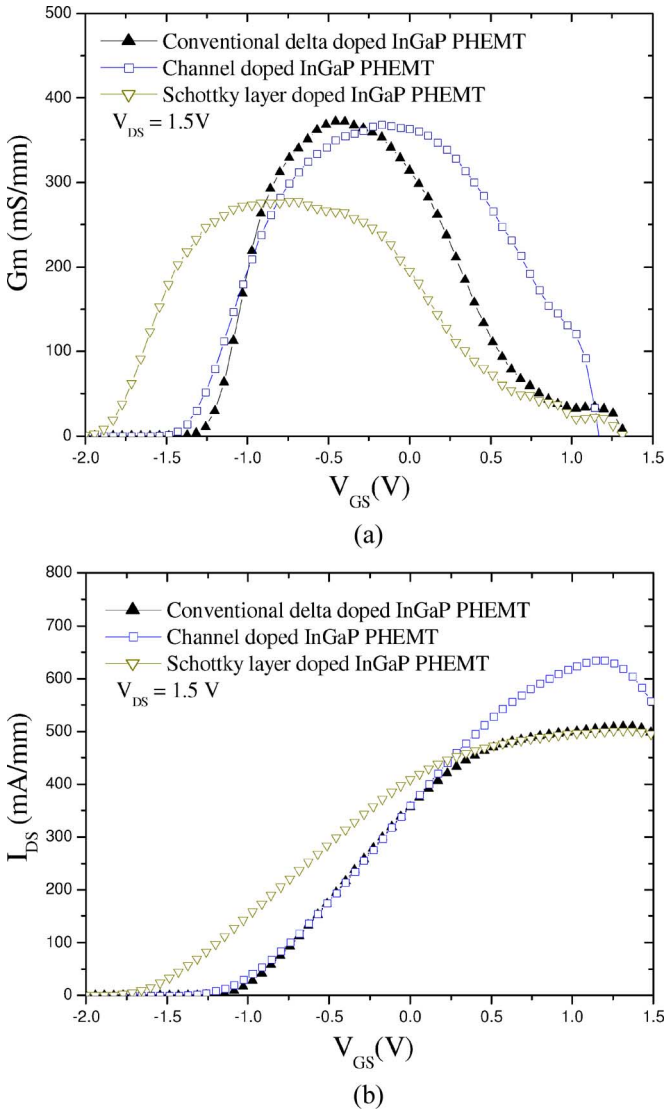

Fig. 4. (a) Gm versus $V_{\rm GS}$ curves and (b) $I_{\rm DS}$ versus $V_{\rm GS}$ curves for the three different types of devices studied, the device size is 0.25×160 μm^2 and the $V_{\rm DS}$ bias is 1.5 V.

IV. Results and Discussion

The three different types of 0.25×160-μm InGaP/InGaAs HEMTs, as shown in Fig. 1, were fabricated, tested, and compared. Fig. 3 shows the $I_{\rm DS}$ versus $V_{\rm DS}$ curves of the three different types of devices. From a comparison of these devices, it can be seen that the Schottky layer-doped device has a higher $I_{\rm DSS}$ ($I_{\rm DS}$ @ $V_{\rm GS}=0$ V) of 408.7 mA/mm and has a higher pinch-off voltage of -1.8 V. The characteristics of the Gm dependence on the gate-bias are shown in Fig. 4(a). It can be observed that extra doping, either in the channel or in the Schottky layer of a conventional δ-doped InGaP/InGaAs pHEMT, result in a flatter Gm distribution, but both have a lower maximum Gm value as compared to that of a conventional δ-doped device. The comparative $I_{\rm DS}-V_{\rm GS}$ curve for these devices is shown in Fig. 4(b). The channel-doped device has the maximum $I_{\rm DS}$ value of 634.3 mA/mm, which is the highest of the three structures. The extra doping in the Schottky layer increases the number of electrons in the 2DEG and results in a higher

TABLE I
COMPARISON OF THE DC CHARACTERISTICS OF THE THREE DIFFERENT TYPES OF DEVICES

Device Type			Conventional doped InGaP/InGaAs PHEMT	Schottky layer doped InGaP/InGaAs PHEMT	Channel doped InGaP/InGaAs PHEMT
Doping density	Delta doping (cm^{-2})	above	4.0×10^{12}	4.0×10^{12}	4.0×10^{12}
		below	2.0×10^{12}	2.0×10^{12}	2.0×10^{12}
	Channel layer(cm^{-3})		undoped	undoped	5.0×10^{17}
	Schottky layer(cm^{-3})		undoped	5.0×10^{17}	undoped
I_{DSS} (I_{DS} @ V_{GS}=0, mA/mm)			356.9	408.7	359.6
I_{DS}-max (mA/mm)			509.3	501.2	634.3
Gm_{max} (mS/mm)			372.1	277.6	368.4
Pinch-off voltage			-1.25	-1.80	-1.35
I_{DS}-V_{GS} polynomial 1st order coefficient a_1			0.04978	0.03079	0.05742
I_{DS}-V_{GS} polynomial 3rd order coefficient a_3			-0.01453	-0.00592	-0.00968
a_3/a_1			-0.29188	-0.19227	-0.16858
I_{DS}-V_{GS} polynomial 5th order coefficient a_5			0.00385	0.00423	0.00015
a_5/a_1			0.07734	0.13738	0.00261

$I_{\rm DSS}$ along with a higher pinch-off voltage. Meanwhile, extra doping in the channel layer results in a more uniform electron distribution in the 2DEG with a higher maximum $I_{\rm DS}$ value, but the $I_{\rm DSS}$ and pinch-off voltage remain the same as that of the device without extra doping.

However, both Schottky barrier doping and channel doping increase the gate-leakage current of the devices. The addition of doping typically reduces breakdown voltages, indicating that the extra doping can improve the device linearity and can be used for handset applications. However, it is not preferred in high-voltage operations of base stations. A comparison of the dc characteristics of these three 0.25 × 160-μm devices is presented in Table I.

To further investigate the linearity performance of the three devices, the polynomial curve-fitting technique, using (10), was applied to the transfer characteristic functions of these devices.

Moreover, the IM3 levels incurred by the device can then be readily derived as [11] and [12]

$$\text{IM3} = \frac{3}{8}a_3A^3 + \frac{50}{32}a_5A^5. \tag{13}$$

For a device with good linearity, $I_{\rm DS}$ should increase linearly with $V_{\rm GS}$, therefore, a_1 should be larger and the higher order constants a_3 and a_5 should be minimized [12]. The coefficients of these devices extracted from the measurement data when $V_{\rm DS} = 1.5$ V are listed in Table I. From a comparison of the data of these three different devices in Table I, it can be clearly observed that the channel-doped device has a larger a_1 and smaller a_3 and a_5 values, while the Schottky layer-doped device only shows lower a_3.

To evaluate the device linearity, the IM3 level and IP3 of these devices were measured. The IM3 and IP3 measurements were carried out by injecting two signals with the same amplitude but at two different frequencies: 5.8 and 5.801 GHz, setting the devices biased at $V_{\rm DS} = 1.5$ V, and adjusting the $I_{\rm DS}$ to get the IP3 versus $I_{\rm DS}$ curves. Fig. 5 shows the IP3 versus $I_{\rm DS}$ curves of these three different 0.25 × 160-μm devices, which had their individual load impedances tuned for maximum power. It also shows that the two devices with extra doping have higher IP3 values. Moreover, while the channel-doped

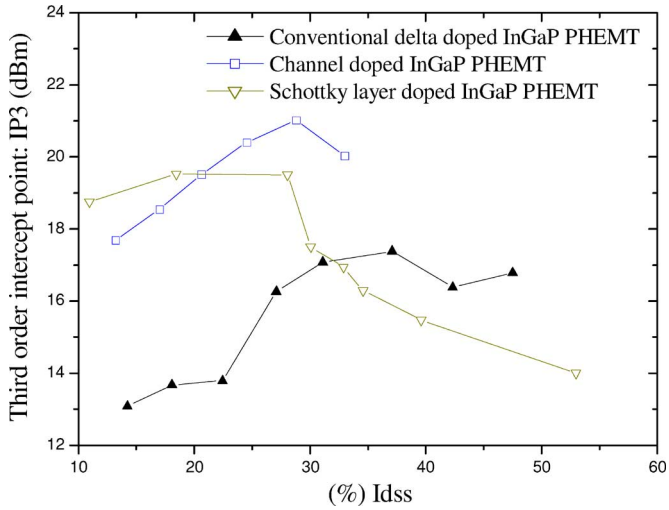

Fig. 5. IP3 versus $I_{\rm DS}$ curves of the three 0.25 × 160-μm^2 InGaP/InGaAs pHEMTs in this paper, the test frequency is 5.8 GHz and $V_{\rm DS} = 1.5$ V.

device has a high IP3 over a wider region versus different $I_{\rm DS}$, the Schottky layer-doped device has a high IP3 in the lower $I_{\rm DS}$-bias region. The measured maximum IP3 for these devices are listed in Table II. The $\Gamma_{\rm source}$ and $\Gamma_{\rm load}$ tuning of the conventional δ-doped, Schottky layer-doped, and channel-doped devices are $0.50^\circ\angle 56.7^\circ$ and $0.46^\circ\angle 47.7^\circ$, $0.05^\circ\angle -176.17^\circ$ and $0.58^\circ\angle 32.3^\circ$; and $0.52^\circ\angle 99.9^\circ$ and $0.51^\circ\angle 56.0^\circ$, respectively. The channel-doped device shows a higher IP3 of 21.02 dBm, a higher Δ (IP3 $- P_{1\ \rm dB}$) of 14.23 dB, and a higher IP3 to dc power consumption ratio (IP3/$P_{\rm DC}$) of 4.97 when compared to those of the other devices. Overall, the channel-doped device has the highest figure of merit value for device linearity. Fig. 6 shows the IM3 value of these three devices with the DC-bias point at the maximum IP3 condition. The measured IM3 levels at 20 dB, backed off from $P_{1\ \rm dB}$, are also included in Table II. Much lower IM3 levels for the devices with extra doping were observed when compared to those of the conventional δ-doped device, particularly, for the channel-doped device (-82 dBm). From the data in Figs. 4–6, it can be concluded that extra doping, either in the channel region or in the Schottky layer, can achieves a flatter Gm distribution versus

TABLE II
COMPARISON OF THE IM3 AND IP3 OF THE THREE DIFFERENT TYPES OF DEVICES

Device Type	DC bias point: V_{DS} = 1.5V					
		Operation frequency: 5.8GHz				
	I_{DS} (mA)	IM3 level at 20dB back-off from P_{1dB} (dBm)	P1dB (dBm)	IP3 (dBm)	Δ (IP3-P1dB) (dB)	IP3/PDC
Conventional delta-doped InGaP/InGaAs PHEMT	22.34	-75	5.79	17.38	11.59	1.63
Schottky layer doped InGaP/InGaAs PHEMT	14.72	-80	5.43	19.52	14.10	4.06
Channel doped InGaP/InGaAs PHEMT	16.96	-82	6.79	21.02	14.23	4.97

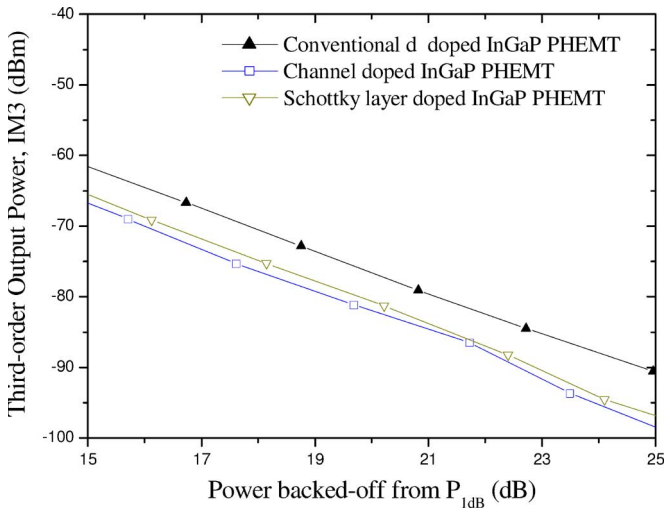

Fig. 6. IM3 versus power backed off from $P_{1\,\mathrm{dB}}$ curves for the three different types of InGaP/InGaAs pHEMTs, device size: 0.25 × 160 μm^2, test condition: $V_{\mathrm{DS}} = 1.5$ V, I_{DS} bias at maximum IP3, and the input signal frequency is 5.8 GHz.

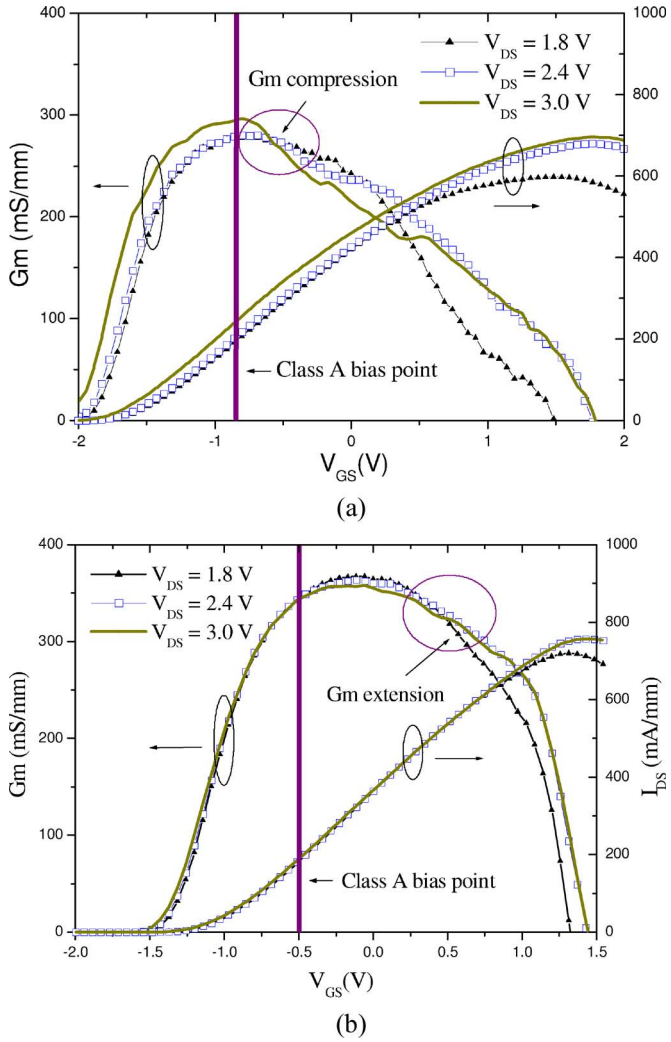

Fig. 7. Gm versus V_{GS} curves at different V_{DS} bias points for (a) Schottky layer-doped device and (b) channel-doped device.

V_{GS} bias. Moreover, extra doping in the channel region or in the Schottky layer results in a lower overall IM3 level and higher IP3 value for these devices, while the same condition result in a higher peak Gm value in a conventional δ-doped device.

To further analyze the effects of Gm distribution with different doping modifications, the Gm distributions versus different V_{DS} were also compared for the Schottky layer-doped and channel-doped devices. Fig. 7 shows the Gm versus V_{GS} distribution curves of these devices under different drain-to-source voltage (V_{DS}) biases. The Gm distribution became sharper for the Schottky layer-doped device and more gradual for the channel-doped device as the V_{DS} bias increased, as shown in Fig. 7(a) for the Schottky layer-doped device and Fig. 7(b) for the channel-doped device. These results show that the extra doping in the different layers of the devices results in different electron distributions. The channel-doped device shows a more uniform electron distribution in the 2DEG when the V_{DS} bias increases.But for the Schottky layer-doped device, the electrons concentration is higher at the top of the channel where the electron distribution is sharp on one side. A load-pull measurement was performed on these devices using a wideband-code-division multiple-access (W-CDMA) modulation signal as the input to evaluate the device linearity at different dc biases. The $P_{1\,\mathrm{dB}}$, gain, and power-added efficiency (PAE) of these devices were measured by using a single-tone input power at 5.8 GHz and by tuning the maximum power with different V_{DS} at the best biases for IM3 level. A W-CDMA modulation signal was used as the input signal to meet the adjacent-channel power ratio (ACPR) with $P_{1\,\mathrm{dB}}$ at ±5-MHz offset and at ±10-MHz offset from the center frequency. Table III shows a comparison of the ACPR measurements for both the Schottky layer-doped device and the channel-doped device under different V_{DS} biases at the best I_{DS} bias for the IM3. As shown in Fig. 7, as a

TABLE III
COMPARISON OF ACPR OF THE SCHOTTKY LAYER-DOPED DEVICE AND THE CHANNEL-DOPED DEVICE UNDER DIFFERENT $V_{\rm DS}$ AT THE BEST $I_{\rm DS}$ BIAS FOR IM3

Device	RF Performance		The best I_{DS} bias for IM3	
			V_{DS}=1.5	V_{DS}=3.0
Schottky layer doped InGaP/InGaAs PHEMT	ACPR (dBc)	Pout(dBm)	-27.58	-24.15
		+5MHz offset	-30.44	-29.24
		-5MHz offset	-30.31	-25.70
		+10MHz offset	-52.59	-50.57
		-10MHz offset	-52.59	-48.29
Channel doped InGaP/InGaAs PHEMT	ACPR (dBc)	Pout(dBm)	-28.01	-22.88
		+5MHz offset	-30.54	-32.69
		-5MHz offset	-29.98	-30.38
		+10MHz offset	-51.66	-52.42
		-10MHz offset	-52.39	-52.33

TABLE IV
$P_{1\ \rm dB}$, GAIN, PAE, AND ACPR OF THE THREE DIFFERENT DEVICES UNDER DIFFERENT $V_{\rm DS}$ AT CLASS-A-BIAS

Device	RF Performance		Class A		
			V_{DS} =1.5	V_{DS} =2.4	V_{DS} =3.0
Schottky layer doped InGaP/InGaAs PHEMT	P1dB(dBm)		7.58	9.25	11.47
	Gain(dB)		20.11	21.98	22.49
	PAE(%)		9.55	8.76	11.41
	ACPR (dBc)	+5MHz offset	-28.75	-28.33	-21.37
		-5MHz offset	-30.19	-28.28	-22.82
		+10MHz offset	-47.28	-48.06	-38.84
		-10MHz offset	-51.20	-49.75	-41.64
Channel doped InGaP/InGaAs PHEMT	P1dB(dBm)		8.17	12.48	14.20
	Gain(dB)		13.63	13.89	14.01
	PAE(%)		15.08	25.43	29.23
	ACPR (dBc)	+5MHz offset	-32.30	-37.03	-40.96
		-5MHz offset	-32.43	-36.58	-40.17
		+10MHz offset	-51.40	-54.63	-55.39
		-10MHz offset	-53.05	-54.75	-55.19

result of the bias point being on the left-hand side of the Gm profile ($V_{\rm GS} < 0$), the Gm distribution is similar with different $V_{\rm DS}$ biases. Therefore, the ACPR value was found in this paper show only a small variation with changes to the $V_{\rm DS}$ bias. More specifically, for the channel-doped device, the ACPR measurement improves as the $V_{\rm DS}$ bias increases, while for the Schottky layer-doped device, the ACPR measurement declines with increase in $V_{\rm DS}$ bias (these results are consistent with the Gm profiles in Fig. 7). Table IV presents a summary of the device power performances and the ACPR values when the two devices were Class-A-biased. The channel-doped device shows a higher $P_{1\ \rm dB}$ with a higher PAE. Because the bias point is close to the peak of the Gm profile, the Gm distribution changes as the $V_{\rm DS}$ bias increases. When the $V_{\rm DS}$ bias point increases, the adjacent-channel leakage power of the channel-doped device decreases while the Schottky layer-doped device increases. From the above results, it can be further verified that the performance of the ACPR measurement for the devices depends on the Gm profile. A gradual Gm distribution results in a higher ACPR value than a sharp Gm distribution. The δ-doped InGaP/InGaAs pHEMT with lightly doping in the channel results in a flatter Gm distribution, and the flatness of the Gm distribution continues to extend as the $V_{\rm DS}$ bias increases. However, for the Schottky layer-doped device, the distribution of Gm is compressed with an increase $V_{\rm DS}$ bias. The ACPR tests performed on these two devices using 5.8-GHz W-CDMA modulation signals, and a $V_{\rm DS}$ bias at 3 V are shown in Fig. 8. The channel-doped device performs better power performance with a $P_{1\ \rm dB}$ of 14.20 dBm, PAE of 29.23%, and ACPR of -40 dBc at $\pm$5-MHz offset and -55 dBc at $\pm$10-MHz offset from the center frequency [Fig. 8(a)]. The performance of the Schottky layer-doped device is inferior to that of the channel-doped device as it only obtained a $P_{1\ \rm dB}$ of 11.47 dBm, PAE of 11.41%, and ACPR of -21 dBc at $\pm$5-MHz offset and -38 dBc at $\pm$10-MHz offset [Fig. 8(b)]. By contrast, the channel-doped device demonstrates a much better linearity under CDMA modulation than does the Schottky layer-doped device, particularly, if there is a high $V_{\rm DS}$ bias.

V. CONCLUSION

The improved device linearity of the δ-doped InGaP/InGaAs pHEMTs with extra doping has been demonstrated. The extra doping, either in the channel layer or in the Schottky layer,

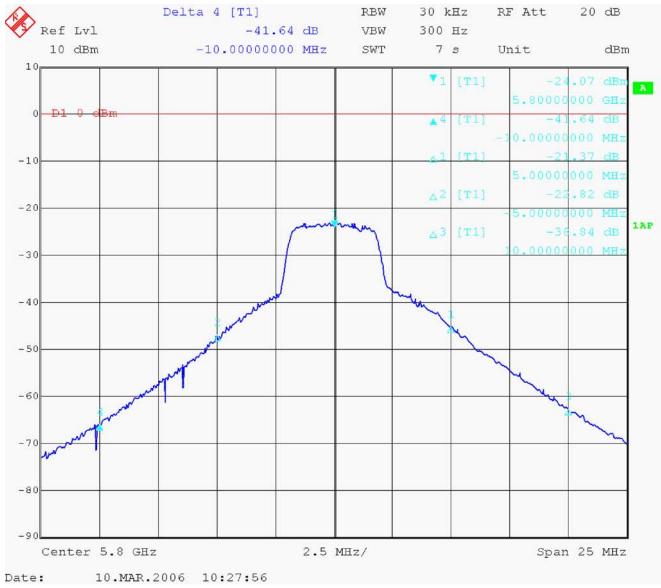

(a)

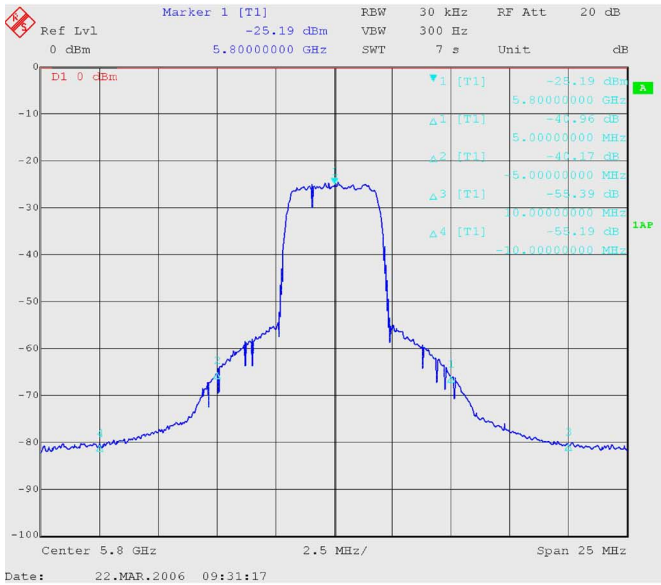

(b)

Fig. 8. ACPR spectrum of the InGaP/InGaAs pHEMTs. (a) Schottky layer-doped device. (b) Channel-doped device. Device size: $0.25 \times 160\ \mu m^2$, test condition: $V_{DS} = 3$ V, class-AB bias, and the input signal frequency is 5.8 GHz.

results in the increased flatness of the Gm versus V_{GS} curve and also leads to lower overall IM3 level and higher IP3 value for these devices even though the conventional device exhibits higher peak Gm. After a light doping of $5 \times 10^{17}/cm^3$ in the channel region, the channel-doped device, when compared to the other two devices, achieved the maximum I_{DS}, the flattest Gm versus V_{GS}, and a Gm value which increased with an increase in V_{DS} bias. Furthermore, although the channel-doped device has the lowest electron mobility, the dc characteristics have caused it to have the highest IP3 value and the lowest IM3 level, as well as the best ACPR value during CDMA modulation. The experimental results presented in this paper are consistent with the accompanying theoretical analyses. In summary, doping modification, either in the channel region or in the Schottky layer, has been proven to be effective in the improvement of the linearity of InGaP/InGaAs pHEMT devices. In short, this approach can be used in the development of high-linearity devices for application in wireless-communication technology.

REFERENCES

[1] E. Lan, E. Johnson, B. Knappenberger, and M. Miller, "InGaP pHEMTs for 3.5 GHz W-CDMA applications," in *Proc. IEEE MTT-S Dig.*, 2002, vol. 2, pp. 1039–1042.

[2] M. Y. Kao, E. A. Beam, III, P. Saunier, and W. R. Frensley, "X-band InGaP pHEMTs with 70% power-added efficiency," in *Proc. IEEE MTT-S Dig.*, 1998, vol. 3, pp. 1671–1674.

[3] Y. C. Lin, E. Y. Chang, G. J. Chen, H. M. Lee, G. W. Huang, D. Biswas, and C. Y. Chang, "InGaP/InGaAs pHEMT with high IP3 for low noise applications," *Electron. Lett.*, vol. 40, no. 11, pp. 777–778, 2004.

[4] K. Y. Hur, K. T. Hetzler, R. A. McTaggart, D. W. Vye, P. J. Lemonias, and W. E. Hoke, "Ultralinear double pulse doped AlInAs/GaInAs/InP HEMTs," *Electron. Lett.*, vol. 32, no. 16, pp. 1516–1517, 1996.

[5] P. P. Ruden, M. Shur, A. I. Akinwande, J. C. Nohava, D. E. Grider, and J. Baek, "AlGaAs/InGaAs/GaAs quantum well doped channel heterostructure field effect transistors," *IEEE Trans. Electron Devices*, vol. 37, no. 10, pp. 2171–2175, Oct. 1990.

[6] R. S. Tucker, "Third-order intermodulation distortion and gain compression in GaAs FETs," *IEEE Trans. Microw. Theory Tech.*, vol. MTT-27, no. 5, pp. 400–408, May 1979.

[7] M. J. Bailey, "Intermodulation distortion in pseudomorphic HEMT's and an extension of the classical theory," *IEEE Trans. Microw. Theory Tech.*, vol. 48, no. 1, pp. 104–110, Jan. 2000.

[8] A. M. Crosmun and S. A. Maas, "Minimization of intermodulation distortion in GaAs MESFET small-signal amplifiers," *IEEE Trans. Microw. Theory Tech.*, vol. 37, no. 9, pp. 1411–1417, 1989.

[9] J. C. Pedro and J. Perez, "Accurate simulation of GaAs MESFET's intermodulation distortion using a new drain-source current model," *IEEE Trans. Microw. Theory Tech.*, vol. 42, no. 1, pp. 25–33, 1994.

[10] C. Gaquiere, F. Bue, P. Delemotte, Y. Crosnier, B. Carnez, and D. Pons, "Effects on the linearity in Ka band of single or double-recessed pHEMTs," *IEEE Microw. Guided Wave Lett.*, vol. 10, no. 7, pp. 267–269, Jul. 2000.

[11] N. B. de Carvalho and J. C. Pedro, "Large- and small-signal IMd behavior of microwave power amplifiers," *IEEE Trans. Microw. Theory Tech.*, vol. 47, no. 12, pp. 2364–2374, Dec. 1999.

[12] H. C. Chiu, S. C. Yang, F. T. Chien, and Y. J. Chan, "Improved device linearity of AlGaAs/InGaAs HFETs by a second mesa etching," *IEEE Electron Device Lett.*, vol. 23, no. 1, pp. 1–3, Jan. 2002.

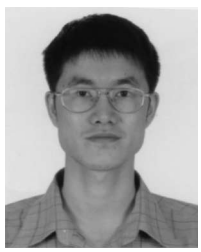

Yueh-Chin Lin was born in Taipei, Taiwan, R.O.C. He received the B.S. degree in nuclear engineering and engineering physics and the M.S. degree in electrical engineering from Tsing Hua University, Hsinchu, Taiwan, R.O.C., in 1996 and 2000, respectively, and the Ph.D. degree from materials science and engineering, National Chiao Tung University (NCTU), Hsinchu, in 2006.

From 2004 to 2006, he was with NTT Basic Research Laboratories, where he investigated the growth of AlGaSb/InAs HEMT on Si substrate by molecular beam epitaxy (MBE). He is currently a Postdoc in the Department of Materials Science and Engineering and Microelectronics and Information Systems Research Center, NCTU. His research interests include MBE material growth and HEMT device design and fabrication for wireless communication.

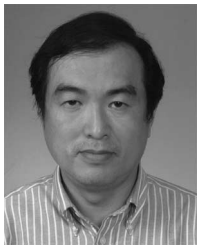

Edward Yi Chang (S'85–M'85–SM'04) received the B.S. degree from the Department of Materials Science and Engineering, National Tsing Hua University, Hsinchu, Taiwan, R.O.C., in 1977, and the Ph.D. degree from the Department of Materials Science and Engineering, University of Minnesota, Minneapolis, in 1985.

From 1985 to 1988, he was with Unisys Corporation GaAs Component Group, Eagan, MN, and Comsat Labs Microelectronic Group from 1988 to 1992. He worked on the GaAs MMIC programs on both groups. He was with National Chiao Tung University (NCTU), Hsinchu, Taiwan, R.O.C., in 1992. In 1994, he helped set up the first GaAs MMIC production line in Taiwan and become president of Hexawave Inc., Hsinchu, in 1995. He returned to the teaching position at NCTU in 1999 and is currently the Head and Professor in the Department of Materials Science. His research interests include new device and process technologies for compound semiconductor RFICs for wireless communication.

Dr. Chang is a senior member and a Distinguished Lecturer of the IEEE Electronic Device Society.

Hiroshi Yamaguchi was born in Osaka on October 30, 1961. He received the B.E. degree in engineering, the M.S. degree in physics, and the Ph.D. degree in engineering from Osaka University, Osaka, Japan, in 1984, 1986, and 1993, respectively.

He was with NTT Basic Research Laboratories in 1986. He was a Visiting Research Fellow at the Imperial College, University of London, U.K., during 1995–1996. Since 1986, he has been engaged in the study of compound semiconductor surfaces prepared by molecular beam epitaxy mainly using electron diffraction and scanning tunneling microscopy. His current interests are in mechanical and elastic properties of semiconductor low dimensional structures. He was a Research Coordinator of NEDO international joint research project (nanoelasticity) during 2001–2004, and also a Guest Professor with the Department of Physics, Tohoku University since 2005.

Dr. Yamaguchi was a member of the Japan Society of Applied Physics and the Physical Society of Japan. He was the recipient of the paper awards from the Japanese Society of Applied Physics in 1989 and 2004.

Wei-Cheng Wu was born in Hsinchu, Taiwan, R.O.C., in 1979. He received the B.S. degree from the Department of Materials Science and Engineering, National Chiao Tung University, Hsinchu, in 2001. He is currently working toward the dual Ph.D. degrees in materials science and engineering at the National Chiao Tung University and at the Department of Microtechnology and Nanoscience, MC2, Chalmers University of Technology, Göteborg, Sweden.

His research interests include fabrication, characterization, and packaging technologies of compound semiconductor devices and ICs for high-frequency applications, particularly flip-chip interconnect and transition design.

Chun-Yen Chang (S'69–M'70–SM'81–F'88–LF'05) was born in Feng-Shan, Taiwan, R.O.C. He received the B.S. degree in electrical engineering from Cheng Kung University, Tainan, Taiwan, R.O.C., in 1960, and the M.S. degree in tunneling in semiconductor–supercondutor junctions and the Ph.D. degree in carrier transport across metal-semiconductor barrier from the National Chiao Tung University (NCTU), Hsinchu, Taiwan, R.O.C., in 1969.

He has devoted himself to education and academic research for more than 40 years. He has contributed profoundly to the areas of microelectronics and optoelectronics, including the invention of the method of low-pressure MOCVD using triethyl-gallium to fabricate LED, laser, and microwave transistors, Zn-incorporation of SiO for stabilization of power devices, and nitridation of SiO for ultra large-scale integrations, etc. From 1962 to 1963, he fulfilled his military service by establishing at NCTU Taiwan's first experiment TV transmitter that formed the founding structure of today's Chinese Television Service. In 1963, he was with NCTU to serve as an Instructor establishing a high-vacuum laboratory. In 1964, he and his colleague established the semiconductor research center at NCTU with a very up-to-date, albeit homemade, facility for silicon-device processing, where they made the nation's first Si Planar transistor in April 1965 and, subsequently, the first IC in August 1966. In 1968, he published Taiwan's first-ever semiconductor paper in the *International Journal Solid State Electronics*. In 1969, he became a Full Professor, teaching solid state physics, quantum mechanics, semiconductor devices, and technologies. From 1977 to 1987, he single-handedly established a strong electrical engineering and computer science program at NCTU, where GaAs, Si, and poly-Si researches were established in Taiwan for the first time. Since 1987, he served consecutively as Dean of Research (1987–1990), Dean of Engineering (1990–1994), and Dean of Electrical Engineering and Computer Science (1994–1995). Simultaneously, he was serving as the founding President of the National Nano Device Laboratories from 1990 to 1997. In 1997, he became Director of the Microelectronics and Information System Research Center, NCTU (1997–1998). Many of his former students have since become founders of the most influential hi-tech enterprises in Taiwan, namely, UMC, TSMC, Winbond, MOSEL, Acer, Leo, etc. In August 1, 1998, he was appointed as the President of NCTU (1998–2006). As the National Chair Professor and President of NCTU, his vision is to lead the university for excellence in engineering, humanity, art, science, management, and biotechnology. To strive forward to world-class multidisciplinary university is the main goal to which he and his colleagues have committed.

Dr. Chang was the recipient of the IEEE Third Millennium Medal in 2000. He is a member of Academia Sinica and a Foreign Associate of the National Academy of Engineering.